

# CM<sup>2</sup>



# MAGAZINE

第 17 期



南方科技大学海洋磁学中心主编

# 创刊词

海洋是生命的摇篮，是文明的纽带。地球上最早的生命诞生于海洋，海洋里的生命最终进化成了人类，人类的文化融合又通过海洋得以实现。人因海而兴。

人类对海洋的探索从未停止。从远古时代美丽的神话传说，到麦哲伦的全球航行，再到现代对大洋的科学钻探计划，海洋逐渐从人类敬畏崇拜幻想的精神寄托演变成可以开发利用与科学研究的客观存在。其中，上个世纪与太空探索同步发展的大洋科学钻探计划将人类对海洋的认知推向了崭新的纬度：深海（deep sea）与深时（deep time）。大洋钻探计划让人类知道，奔流不息的大海之下，埋藏的却是亿万年的地球历史。它们记录了地球板块的运动，从而使板块构造学说得到证实；它们记录了地球环境的演变，从而让古海洋学方兴未艾。

在探索海洋的悠久历史中，从大航海时代的导航，到大洋钻探计划中不可或缺的磁性地层学，磁学发挥了不可替代的作用。这不是偶然，因为从微观到宏观，磁性是最基本的物理属性之一，可以说，万物皆有磁性。基于课题组的学科背景和对海洋的理解，我们对海洋的探索以磁学为主要手段，海洋磁学中心因此而生。

海洋磁学中心，简称  $CM^2$ ，一为其全名“Centre for Marine Magnetism”的缩写，另者恰与爱因斯坦著名的质能方程  $E = MC^2$  对称，借以表达我们对科学巨匠的敬仰和对科学的不懈追求。

然而科学从来不是单打独斗的产物。我们以磁学为研究海洋的主攻利器，但绝不仅限于磁学。凡与磁学相关的领域均是我们关注的重点。为了跟踪反映国内外地球科学特别是与磁学有关的地球科学领域的最新研究进展，海洋磁学中心特地主办  $CM^2$  Magazine，以期与各位地球科学工作者相互交流学习、合作共进！

“海洋孕育了生命，联通了世界，促进了发展”。21世纪是海洋科学的时代，由陆向海，让我们携手迈进中国海洋科学的黄金时代

# 目 录

海磁文苑.....	1
我的科研观.....	1
岩石磁学演绎.....	5
第 7 章 磁化率概念进三阶.....	5
文献导读.....	8
1. 南大洋不同水团对于冰消期大气 CO <sub>2</sub> 升高的贡献各不相同	8
2. 富 <sup>18</sup> O 的早太古代海洋反映了太古宙有限的陆壳出现...	11
3. 早新元古代磷制约的海洋环境维持了较低大气氧含量..	13
4. 晚新生代东南极洲和西南极洲的聚合.....	16
5. 湖泊沉积物中碳酸盐岩的稳定氧碳同位素作为古洪水的代 用指标.....	19
6. 海洋中金属元素在生物和非生物作用下的滞留、再循环和矿 化过程.....	22
7. 中国降水的稳定同位素组成.....	24
8. 全新世以来南海北部海岸海表温度变化所指示的亚洲冬季 季风记录.....	27

## 我的科研观

杨会会

“我的科研观”首先要来说说“科研”，什么是现代科学研究、地学研究。这要参考客观解释和我为数不多的科研经历，当然也反映了我的价值观和我未来的职业选择。

“计算科学（数值模拟）、理论科学（理论分析）和实验科学鼎足而立，是现代科学研究的三大支柱。理论科学是提出论题；实验科学按照理论科学提出的论题进行反复实验，最终得到该理论是否成立的结论；计算科学则是在理论和实验的过程中进行论证与修正”。以上援引自网上对现代普遍科学研究的解释。

对于地学研究而言，“将今论古”无疑是最为重要的方法论，地球科学领域的研究以前人研究文献为基础，以野外观测和采样为先锋，以实验测试和各项科学指标为利刃，得理论或假说之果实。很多课程开课第一节必然是回顾本学科发展历史。在我的印象中，近代早期的地学研究几乎都是西方伯爵之类的全才型知识分子，凭着对自然的好奇和热忱，进行了大量的野外观测，总结成理论，然后发展成学科，为后来者提供了重要的研究资料和理论支持。

有老师曾言，现在的科学研究，包括地学研究，有着明显的职业化，团队化和科技化的倾向。单打独斗的时代已经过去，一批以科学研究为职业的科学家，运用现有的高科技手段，进行各个大方向、小专业，直至微小课题的研究，并不断地在大范围、小范围的交流中，碰撞出进步的火花，推进各自领域的研究向前发展。据说中国的科研队伍一直在迅速地扩大，全职研究人员总数超过美国，科研投入经费也逐年上涨。尽管高质量论文数量，大学排名和专利数量等指标和世界科学中心美帝相比，还有着云泥般的差距，但是跟过去相比，我们已经取得了很大的进步。况且，我一直十分认同中华民族是个勤劳的民族这个说法，干什么都很拼。罗马不是一天建成的，美帝也不是一天能超越的，我们逆流而上，必然道阻且长。虽然这些冠冕堂皇的话由我这个科研小白来说，感觉怪怪的，但是小人物也有大志向，这毕竟代表了我看好祖国发展的一种心态。

说完了大方向，再来说说“我的科研观”。我的老公师兄杨同学在博士阶段研究的是西宁盆地的磁性地层研究。2017年我上硕士，和他一起泡在 PGL 小半年，我用 760 热退，他用 RAPID 交变+热退。屏蔽室冷气吹拂的日子，不知道经历过日夜烧砖的同学回想起来还会不会瑟瑟发抖。

有一天照常夜班上工，我做实验磨得没了脾气，在 760 的“吱吱吱”中问杨同学：“你说咱们天天干这些有啥意义，我吧，好歹是个新剖面，不管做出什么都有话说，你呢？西宁盆地的文章那么多了，你还做，还做得这么艰辛”。他完全不理睬我质疑他的研究创新性不足，回答：“那你做了这个剖面，得到了一些指标，发了一篇或几篇文章，然后呢？”，“然后？然后根据结果和周围同时段其他文章进行区域对比分析啊，或者看看别人在做什么，能不能在这个剖面做做看”，“这就是了，我们俩做的工作是一样的，只是我这儿研究区的研究比你成熟，做的人比较多，前几年有老师在这个研究区给出了一些某时段地层隆升或者下沉的假设，然后大家在互相印证中确认或者推翻这个假设，这就是我现在工作的意义啊。我们硕士博士现阶段能做的就是积累数据而已，有一点创新性即可，而且很多研究人员差不多也是在做这个工作，创新性比硕士博士更强一点，大体上还是为地学的研究做积累和传承工作。聪明上进又走上了科研道路的大牛们也是需要积累的，年轻的时候一边做积累工作一边成长，到四五十岁的时候，知识框架更宏大完整，眼界看向国内外最新最前沿的方向，而且研究经费充足，有能力承担很大的综合又前沿的课题。这时候大牛们有影响力，把控着国内相关领域的研究方向，才算得上为国家做贡献。你还太小又总是太急躁，想要一下子证明自己，你要证明什么，证明给谁看？如果你不改变这个性格，你的科研是做不久的。”这些话在我研究生阶段反复听他提到，基本上构成了我的最初的科研观念，直至今今。也非常不幸的是，杨同学看人确实很准，我随后在深入接触科研的过程中就栽在了性格上，起码是部分缘由于此，到现在也没能站起来。

提到我个人的近况，不知道有没有同学经历过这种感受。美好，开心，满足，欲望，笑容等等这些被隔离在我周身的真空层外围，明明那么近，却在我伸手不可及的千万里之外。我以为新的环境新的家人会不一样，然而遗憾的是，阖家欢聚一堂，我却不能借此融入人间，真实的世界属于真实的人，而我仍旧飘忽游离在正常人的感情之外。我的世界是朦胧的，我的故乡在他乡。这种感受我沉浸式

体验了 2 年，焦虑和恐惧是常态，失眠、噩梦和梦魇是常态。同道中人说太痛苦，我只是仍不习惯明明很好理解的知识它怎么就是不往脑子里进；明明计划列表排得满满的，我却坐在屏幕前整日发呆；明明很简单一件事，我怎么就被定住了一般无法下手，心中充满了恐惧和怅然；明明天气那么好，我的全身心却在抗拒我离开房间；明明大家那么好，我却只想着躲起来躲起来，挖个洞躲起来；明明爱人就在身边，我却不停地想着怎样彻底离开他，了结一切。

我暗自感谢这个超长的假期，这种暗自庆幸显然很不道德，一国沦陷于疫情之中，容我一人苟且偷安于一隅。这个假期给了我充分的时间看向自己，审视自己。我托着下巴盯着窗外：“我否定了我存在的正当性，我要怎么办？我该如何自处？”。杨同学一边晾着衣服，一边对我说：“那就重新构建一个你自己”。一语惊醒梦中人，可是道阻且长啊道阻且长，那就请他祝福我吧。感谢他。

目前这种状态必然会影响我的学习状态和未来的职业规划。杨同学毕业的时候，大家都为他离开了很好的科研平台和团队感到遗憾，他自己完全不这么认为。杨同学非常理性，他会评估做科研投入的精力和获得的报酬，包括经济收入和社会地位带来的个人满足感，甚至评估 20 年后他可以拥有的职称和收入，当然包括对应的这 20 年的生活和压力状态。最终，他选择了一个相对轻松且喜欢的工作，用他的话说即：“我离开科研行业，也可以为国家做贡献啊，我没那么喜欢科研，留在这个行业，我自己过得煎熬，行业里不过多一个平庸的科研者罢了，我要到别处去发光散热，只有选择自己喜欢的行业，能在自己行业里做点实事，就算实现了个人价值和社会价值的统一”。听完这话，我恨不得甩他一套表情包“的确有一套”。我身边很多毕业的师兄、师姐、同学选择了工作，理由不乏科研太累没法一直做下去；读完硕博发现科研跟自己考研时想象的科研行业不一样，也就不喜欢了而放弃；行业竞争压力大，读完博后发现留所、留校、找教职很难，不得不面对就业压力而离开了科研高地，下沉到地方做讲师。

我知道这些现实都是存在的，然而我却不是那种根据现实作出反应的人，或者说相对于理性的杨同学，我是个感性的人，不论现实如何，我喜欢的状态是：这个知识好有趣，我还想知道更多；这个文章的观点我喜欢/不喜欢；这个知识是我发现的，我把它揪出来展示给大家。说得虚荣一点就是那种“站在知识的前沿的感觉”，感觉自己在创造知识，在做实事，在为国争光。跟同学聊起天来，面

对“你们搞科研的每天都干些啥”的问题侃侃而谈，告诉他们我们科研从业者在干什么，有什么意义，每当这个时候都会觉得满足感爆棚。我喜欢这种向上的感觉，不停地接触到更优秀的人，不停地提升自己的能力和眼界，一辈子都在成长。感性的人想得更多，我不聪明但我喜欢思考，我想要一步步去见识和思考这个世界存在和运行的方式，奇妙的，精彩纷呈的，不断变化的世界。这样我可以说：我是一个普通人，普通的科研行业从业者，我有着我的职业认同和骄傲。

如果放在病倒以前，职业根本无需规划，大概是如下场景：

杨同学：“你喜欢现在的状态吗？996？”

我摇头晃脑：“大于996也喜欢，不要拦着我，我要遨游在知识的海洋。”

杨同学：“你觉得你目前的状态坚持到退休可以吗？”

我握拳皱眉：“没问题，我还能为了祖国的科研事业奋斗50年。”

杨同学笑：“那好吧，戏精，你怎么样我都支持。”

事过境迁啊物是人非。我还是我，却总觉得少了一魂一魄，那我还是我吗？我的热血凝固了，我的力气封住了，我的灵气散掉了，我还有能力有资格留在科研行业里吗？我有做其他工作的能力吗？你发现了，我并没有答案。不过，我不喜欢Bad Ending，所以我尽力爬起来，不奢求能继续留在科研行业，容我做个正常人就行。

### 第 7 章 磁化率概念进三阶

Bartington 磁化率仪是目前使用最广泛的磁化率测量仪器。Bartington 磁化率仪是以 10 毫升水作为标样标定的。该标样在 SI 单位下的读数为 $-0.9$ ，对应的体积磁化率为 $-0.9 \times 10^{-5}$ 。在 SI 单位系统下，这个值是没有单位的。而对于其他体积为 10 毫升的样品，其体积磁化率值为仪器的读数乘以  $10^{-5}$ 。对于体积不是 10 毫升的样品，则需要对其体积进行归一化，其体积磁化率为仪器读数乘以  $10^{-5}$ ，然后乘以 10，再除以样品的体积（单位为毫升）。

由于 10 毫升水的质量为 10 克，则在 SI 单位下 $-0.9$  的读数对应的质量磁化率为 $-0.9 \times 10^{-8}$ 。在 SI 单位下，这个值的单位为“ $\text{m}^3/\text{kg}$ ”。而对于其他质量为 10 克的样品，其质量磁化率为仪器的读数乘以  $10^{-8}$ ，单位为  $\text{m}^3/\text{kg}$ 。如果样品的质量不是 10 克，则其质量磁化率等于仪器读数乘以  $10^{-8}$ ，然后乘以 10，再除以样品的质量（单位为克）。

此外，卡帕桥系列(KappaBridge)也是测量磁化率的主要仪器，测量精度要比 Bartington 磁化率仪器高。值得注意的是，卡帕桥磁化率仪器测量读数的单位是  $10^{-6}$  SI。但是，卡帕桥磁化率仪的测量频率固定，不能测量频率磁化率。为了克服这一缺点，Agico 公司新近设计的 MFK 磁化率仪可以变换频率，成为新一代磁化率仪器的主打仪器。

SD 颗粒在升温过程中，弛豫时间 $\tau$ 减小，也就是振动加快，在  $T_B$  会发生解阻，从 SD 状态变成 SP 状态，其磁化率会突然增加。温度再进一步增加，就会趋向  $T_C$ ，磁化率急剧下降。这两种性质叠加在一起，就会在  $T_B$  处形成一个磁化率峰。

我们前面已经学过，体积越大的 SD 颗粒，其  $T_B$  值就越大，磁化率峰也就随之向  $T_C$  移动。当  $T_B$  非常接近  $T_C$  时，磁化率会出现一个非常狭窄尖锐的峰，即霍普金森峰（Hopkinson Peak）。

MD 颗粒一般不会出现这种行为。通过磁化率随着温度变化曲线的特征，可以初步判定磁化率的携带者是处于怎样的粒径范围。

与铁磁性物质不同，顺磁性物质的磁化率( $\chi_{\text{para}}$ )随着温度增加而降低，服从居里定律：

$$\chi_{\text{para}} = C/T,$$

其中 C 是常量，可以通过 $\chi_{\text{para}}$  与 1/T 的关系图做线性拟合进行估算。

对于反铁磁性矿物，其磁化率随着温度的变化比较复杂。这类矿物具有大小相等，方向完全相反的两组磁矩。在其尼尔温度之下，沿着磁矩和垂直于磁矩方向，磁化率随温度变化并不一致。在平行方向， $\chi_{//}$ 受到热扰动和外场共同控制。在尼尔温度点， $\chi_{//}$ 最大，温度降低时，由于热扰动影响逐渐降低，它的值也降低。在垂直方向， $\chi_{\perp}$ 由磁矩的偏转引起。因此，它受温度的影响不大。此外， $\chi_{\perp}$ 永远大于 $\chi_{//}$ 。对于随机分布的颗粒，其体磁化率为 $\chi = 1/3\chi_{\perp} + 2/3\chi_{//}$ 。当温度高于尼尔温度时，反铁磁性物质变为顺磁性质物质，随温度继续增加，磁化率服从居里定律而逐渐减小。

在低温(<300 K)，一些磁性矿物存在着特殊的矿相转化点，比如，磁铁矿的 Verwey 转换(120 K)，以及赤铁矿的 Morin 转换(260 K)。因此，可以通过磁化率在这些温度点的剧烈变化特征来判断这些特定磁性矿物的存在。

除了亚铁磁性和反铁磁性，Rochette (1987)系统地研究了顺磁性物质的磁化率和样品所含离子之间的关系。他发现其中  $\text{Fe}^{2+}$ ， $\text{Fe}^{3+}$ 以及  $\text{Mn}^{2+}$ 对顺磁磁化率的贡献最大。经验公式为

$$K_{\text{para}} = 10^{-3}\rho (25.2\text{Fe}^{2+} + 33.4\text{Fe}^{3+} + 33.8\text{Mn}^{2+}) 10^{-6}\text{SI}$$

其中 $\rho$ 是密度 ( $\text{kg/m}^3$ )，离子含量的单位为重量百分比。

在一般的实验室情况下，外加场小于几个 T，顺磁性物质远远不能饱和。因此，其磁化强度与外加场成正比。因此，常常用高场磁化率来估算顺磁的贡献。比如，可以选取 0.5-1 T 之间磁滞回线的线性段来拟合高场磁化率（单位为  $\text{Am}^2/\text{T}/\text{kg} = \text{Am}^2/(796\text{kA}/\text{m})/\text{kg} = \text{m}^3/\text{kg}/796000$ ）。值得注意的是，反铁磁性物质具有较高的矫顽力，在 1 T 很可能没有完全饱和。这种情况，它们也对高场磁化率有贡献。一般情况下可以不考虑这种影响。但是如果需要非常精确地估算顺磁成分，比较可行的方法是首先应用 CBD 溶液把  $\text{Fe}^{3+}$ 的铁氧化物溶解，之后的高场磁化率才能真正代表顺磁性物质的贡献。

与高场磁化率对应的是低场磁化率,也就是通常磁化率仪器所测量的值( $\chi_{\text{bulk}}$ )。它包含两部分:亚铁磁性磁化率( $\chi_{\text{ferri}}$ )以及顺磁性磁化率( $\chi_{\text{para}}$ )。因此,可以通过扣除顺磁成分来估算亚铁磁性矿物对样品磁化率的贡献,即 $\chi_{\text{ferri}} = \chi_{\text{bulk}} - \chi_{\text{para}}$ 。

顺磁性物质的磁化率比较小,比如中国黄土的顺磁磁化率的量级为  $10^{-7} \text{ m}^3\text{kg}^{-1}$ ,而且随着深度的变化较小。所以,在考虑大尺度的磁化率变化时,基本不需要做顺磁性磁化率的校正。但是,当考虑频率磁化率的百分数时,顺磁性磁化率的影响就不能忽略。

比如,对泥河湾湖相沉积物研究表明,过去湖底经历氧化与环境过程。在还原环境下,亚铁磁性矿物被溶解,而顺磁性物质则不会。于是,可以定义一个参数 $\chi_{\text{bulk}}/\chi_{\text{para}}$ 。如果这个值接近 1,说明样品中亚铁磁性物质含量很低,对应着还原环境。反之,这个值越高,说明亚铁磁性物质的含量越高,对应着氧化环境。

## 文献导读

### 1. 南大洋不同水团对于冰消期大气 CO<sub>2</sub> 升高的贡献各不相同



翻译人：仲义 zhongyi@sustech.edu.cn

*A.D. Moy, M.R. Palmer, W.R. Howard et al., Varied contribution of the Southern Ocean to deglacial atmospheric CO<sub>2</sub> rise [J]. Nature Geoscience, 2019, 12(12), 1006-1011.*

**摘要：**冰期-间冰期大气 CO<sub>2</sub> 的改变总的来说受控于海水中碳的变化，而该变化响应于大尺度上大洋生物地球化学和洋流循环的变化。南大洋当前比其他大洋吸收更多的 CO<sub>2</sub>，并对过去 CO<sub>2</sub> 变化调控发挥重要作用。然而，控制冰期-间冰期海洋-大气 CO<sub>2</sub> 交互作用的物理、生物和化学变化仍然不太清楚。本文中，我们使用有孔虫硼同位素和碳同位素和古温度指标来重建过去 25000 年来亚南极表层水的海水 pH 和 CO<sub>2</sub> 分压特征，来探究调控海水 CO<sub>2</sub> 的受控机制。结果显示，在末次盛冰期时该区域的表层水是大气 CO<sub>2</sub> 的汇入区。我们的记录显示生物泵强度和深海 CO<sub>2</sub> 释放到表层水的变化是末次冰消期大气 CO<sub>2</sub> 升高主要因素。这些发现显示上升流的强度和南大洋水团的分布对于调控冰期-间冰期大气 CO<sub>2</sub> 变化具有重要作用。

**ABSTRACT:** Glacial–interglacial changes in atmospheric CO<sub>2</sub> are generally attributed to changes in seawater carbon chemistry in response to large-scale shifts in the ocean’s biogeochemistry and general circulation. The Southern Ocean currently takes up more CO<sub>2</sub> than any other and it is likely to have played a crucial role in regulating past atmospheric CO<sub>2</sub>. However, the physical, biological and chemical variables that control ocean–atmosphere CO<sub>2</sub> exchange during glacial–interglacial cycles are not completely understood. Here we use boron isotopes and carbon isotopes in planktonic foraminifera and an alkenone-based proxy of temperature to reconstruct seawater pH and CO<sub>2</sub> partial pressure in sub-Antarctic surface waters south of Tasmania over the past 25,000 years, and investigate the mechanisms that regulate seawater CO<sub>2</sub>. The new record shows that surface waters in this region were a sink for atmospheric CO<sub>2</sub> during the Last Glacial Maximum. Our reconstruction suggests changes in the strength of the biological pump and the release of deep-ocean CO<sub>2</sub> to surface waters contributed to the last deglacial rise in atmospheric CO<sub>2</sub>. These findings

demonstrate that variations in upwelling intensity and the distribution of Southern Ocean water masses in this sector played a key role in regulating atmospheric CO<sub>2</sub> during the last glacial–interglacial cycle.

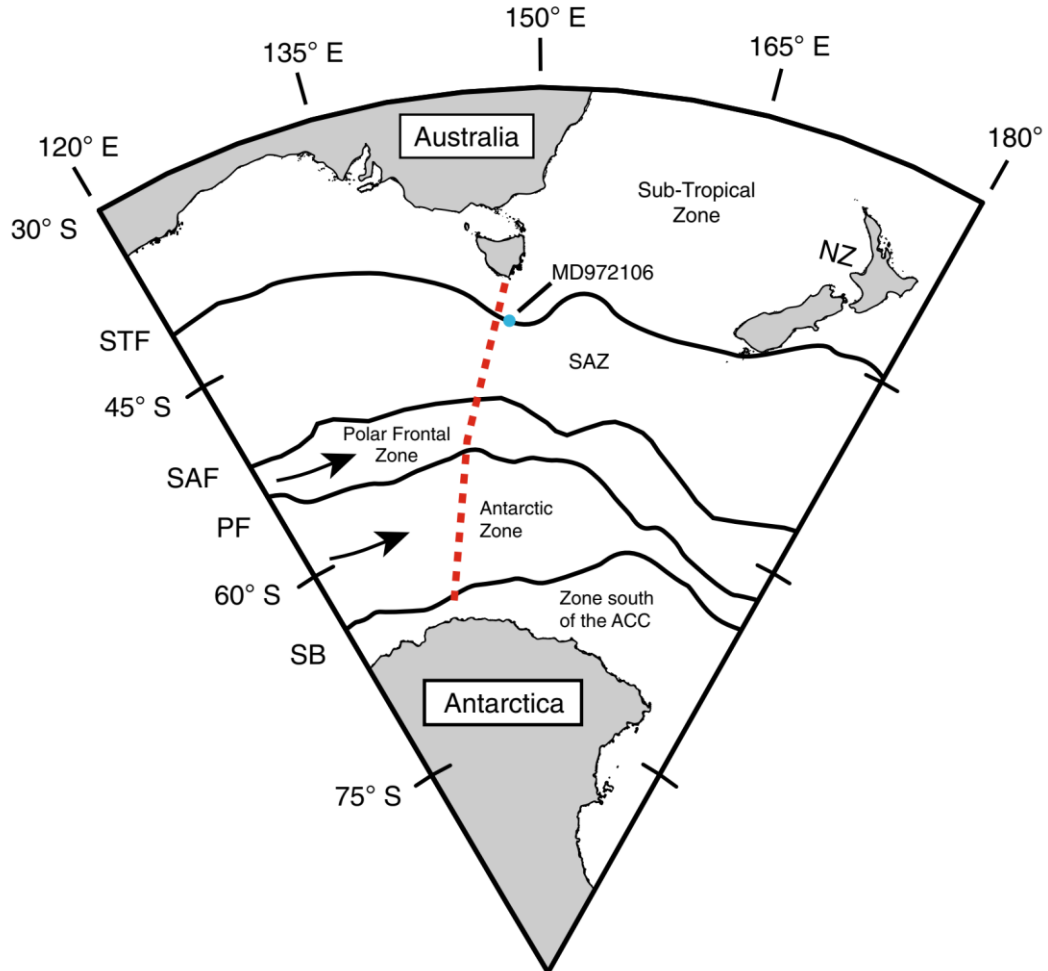


Figure 1. Location of sediment core MD972106 and modern positions of the Southern Ocean water masses and fronts. MD972106 (blue dot) is located at 45° 09' S, 146° 17' E (water depth 3,310 m). SAF, Sub-Antarctic Front; PF, Polar Front; SB, southern boundary of the Antarctic Circumpolar Current (ACC); NZ, New Zealand. Arrows indicate the ACC direction. The dashed red line shows the WOCE SR3 repeat hydrographic transect between Tasmania and Antarctica along ~140° E. Figure adapted from Trull et al.51, John Wiley and Sons.

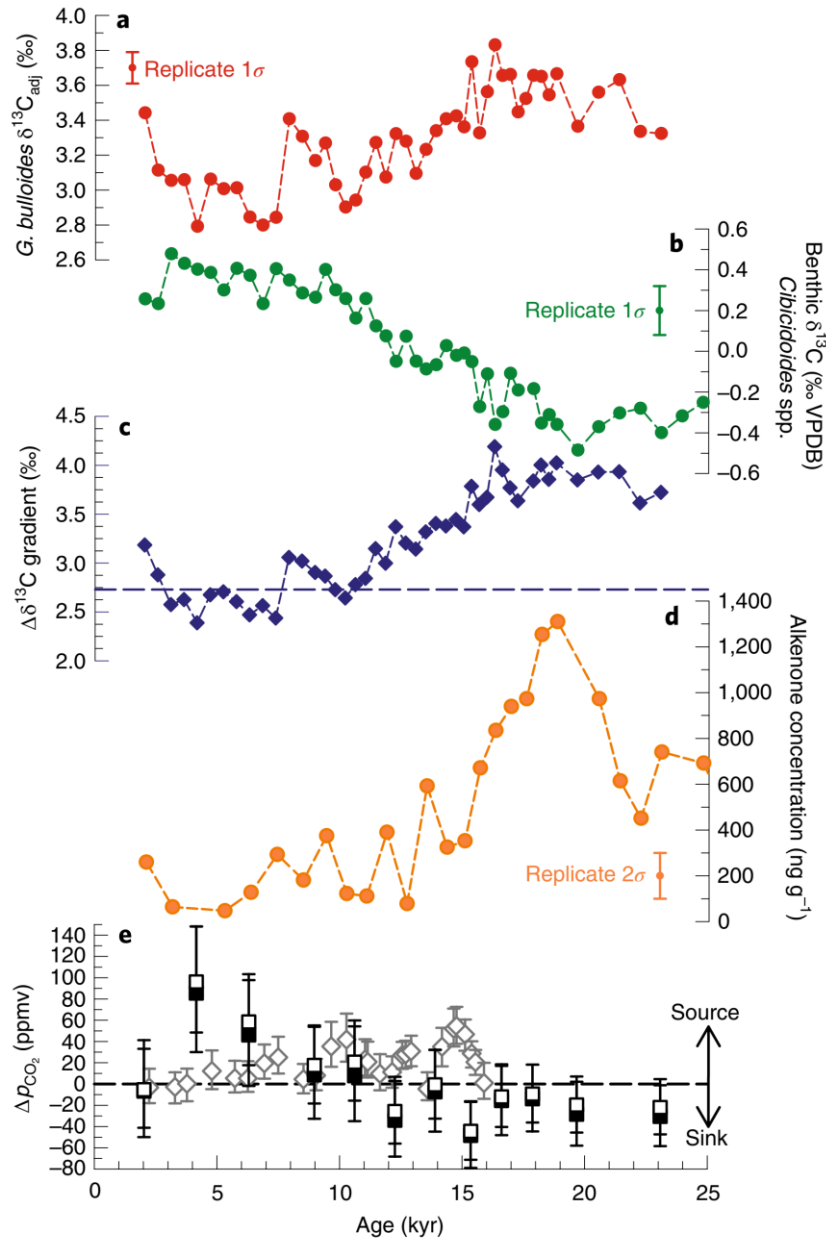


Figure 2. Planktonic and benthic foraminiferal  $\delta^{13}\text{C}$ ,  $\Delta\delta^{13}\text{C}$  gradient, alkenone concentrations and  $\Delta p\text{CO}_2$  over the past 25,000 years. a,  $\delta^{13}\text{C}_{\text{adj}}$  for *G. bulloides*. b, Benthic  $\delta^{13}\text{C}$  for *Cibicidoides* spp. c,  $\Delta\delta^{13}\text{C}$  gradient ( $\delta^{13}\text{C}_{\text{planktonicadj}} - \delta^{13}\text{C}_{\text{benthic foraminifera}}$ ); the horizontal dashed line shows the average Holocene  $\Delta\delta^{13}\text{C}$  gradient. d, Alkenone concentrations. e,  $\Delta p\text{CO}_2$  I is the difference between surface water  $p\text{CO}_2$  I and atmospheric  $p\text{CO}_2$  I (ref. 1) as in Fig. 3c. Also shown in e is the calculated  $\Delta p\text{CO}_2$  I for the Atlantic sector SAZ (ref. 13) (sediment core PS2498-1 at  $44^\circ 09' \text{ S}$ ,  $14^\circ 13' 48'' \text{ W}$ , 3,783 m water depth; the grey open diamonds and error bars are the 95% uncertainty bounds). In a,  $\delta^{13}\text{C}$  values for *G. bulloides* are temperature and  $[\text{CO}_3^{2-}]$  adjusted (Methods). The error bars in a and b represent  $1\sigma$  uncertainties based on replicate measurements, the error bar in d represent  $2\sigma$  uncertainties for replicate extractions and measurements on a homogeneous laboratory standard and the error bars in e represent 95% confidence intervals around the Monte Carlo mean, based on  $2\sigma$  uncertainties on the individual input variables and on other carbonate system parameters propagated via the Monte Carlo simulation ( $n = 10,000$ ) in the program R (Methods)

## 2. 富 $^{18}\text{O}$ 的早太古代海洋反映了太古宙有限的陆壳出现

翻译人: 冯婉仪 [fengwy@sustech.edu.cn](mailto:fengwy@sustech.edu.cn)



Johnson B W, Wing B A. *Limited Archaean continental emergence reflected in an early Archaean  $^{18}\text{O}$ -enriched ocean*[J]. *Nature Geoscience*, 2020, 13: 243-248.

**摘要:** 地球生物圈的起源和进化是由海洋的物理和化学演化历史决定的。海洋化学沉积物和蚀变的洋壳保存了这些演化史的地球化学记录。例如，随着时间的推移，海洋化学沉积物的  $^{18}\text{O}/^{16}\text{O}$  比值逐渐增加。这个信号的含义是模糊的，但是一般反映了两种端员的情况（但两者不是相互排斥的）。如果海洋的氧同位素组成与今天的类似，那么在远古时期的海洋，它的温度可能比现今海洋的温度要高得多。另外，流体-岩石相互作用的性质（包括与大陆形成有关的风化过程）在过去可能有所不同，这导致了海洋氧同位素组成的演变。在这里，我们研究了来自西澳大利亚 Pilbara 克拉通 Panorama 地区的大约 32.4 亿年的热液蚀变洋壳，它可以替代海洋化学沉积物，记录海洋氧同位素的演化。我们发现，在那个时候，Panorama 地区海水的  $\delta^{18}\text{O}$  为  $3.3 \pm 0.1\%$  VSMOW，比现今海洋更富集  $^{18}\text{O}$ 。我们认为海水的  $\delta^{18}\text{O}$  随着时间的推移逐渐降低，这与海洋化学沉积物中记录的  $\delta^{18}\text{O}$  随时间推移呈大幅度增加的趋势不同。为了解释这种可能性，我们建立了一个地质水文循环的氧同位素交换模型，这个模型表明在太古代末期（30 至 25 亿年前），大陆风化作用的开始会导致富  $^{18}\text{O}$  的早太古代海洋的  $\delta^{18}\text{O}$  值下降至类似于现代海水的  $\delta^{18}\text{O}$  值。我们的结论是在大陆出现之前和大陆出现之后，地球的水循环可能经历了两个独立的稳态行为阶段。

**ABSTRACT:** The origin and evolution of Earth's biosphere were shaped by the physical and chemical histories of the oceans. Marine chemical sediments and altered oceanic crust preserve a geochemical record of these histories. Marine chemical sediments, for example, exhibit an increase in their  $^{18}\text{O}/^{16}\text{O}$  ratio through time. The implications of this signal are ambiguous but are typically cast in terms of two endmember (but not mutually exclusive) scenarios. The oceans may have been much warmer in the deep past if they had an oxygen isotope composition similar to that of today. Alternatively, the nature of fluid-rock interactions (including the weathering processes associated with continental emergence) may have been different in the past, leading to an evolving oceanic oxygen isotope composition. Here we examine approximately 3.24-billion-year-old hydrothermally

altered oceanic crust from the Panorama district in the Pilbara Craton of Western Australia as an alternative oxygen isotope archive to marine chemical sediments. We find that, at that time, seawater at Panorama had an oxygen isotope composition enriched in  $^{18}\text{O}$  relative to the modern ocean with a  $\delta^{18}\text{O}$  of  $3.3 \pm 0.1\%$  VSMOW. We suggest that seawater  $\delta^{18}\text{O}$  may have decreased through time, in contrast to the large increases seen in marine chemical sediments. To explain this possibility, we construct an oxygen isotope exchange model of the geologic water cycle, which suggests that the initiation of continental weathering in the late Archaean, between 3 and 2.5 billion years ago, would have drawn down an  $^{18}\text{O}$ -enriched early Archaean ocean to  $\delta^{18}\text{O}$  values similar to those of modern seawater. We conclude that Earth's water cycle may have gone through two separate phases of steady-state behaviour, before and after the emergence of the continents.

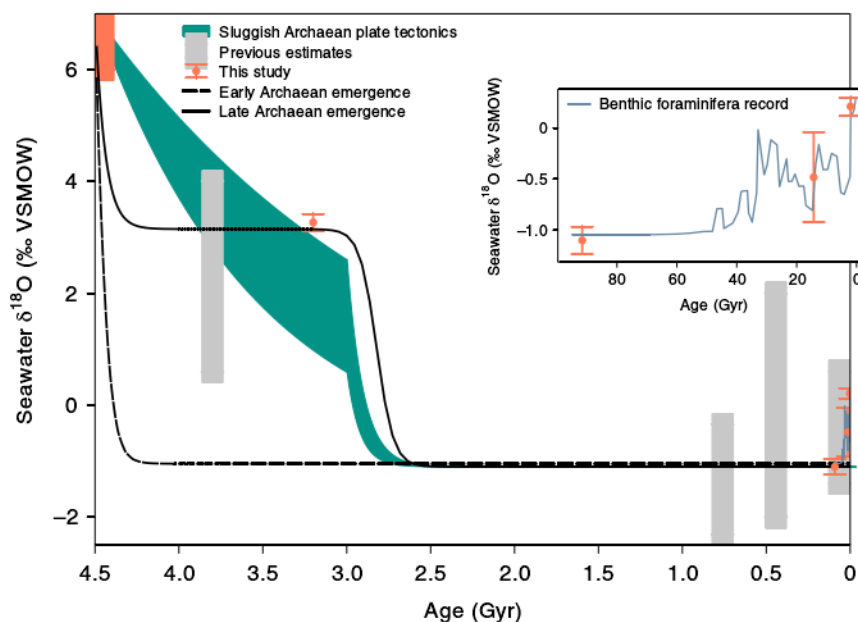


Figure 1. Calculated seawater  $\delta^{18}\text{O}$  evolution for different rate efficiency and continental emergence scenarios. Previous estimates for seawater  $\delta^{18}\text{O}$  from submarine basalts (from oldest to youngest: ref. <sup>41</sup>, ref. <sup>16</sup>, ref. <sup>12</sup>, ref. <sup>13</sup> and ref. <sup>25</sup>) are shown in grey boxes, with our results shown as orange dots (error bars represent two standard deviations). Note the youngest grey box combines two estimates of Phanerozoic seawater  $\delta^{18}\text{O}$ . The constraint at 4.45 Ga (orange box) is based on basaltic magma–water equilibrium<sup>1,42,43</sup> and a bulk Earth  $\delta^{18}\text{O} = 5.5\%$ . The inset shows estimated seawater  $\delta^{18}\text{O}$  for the Cenozoic and the latest Mesozoic based on benthic foraminiferal oxygen isotopes and Mg/Ca ratios<sup>29</sup>. The green field indicates sluggish Archaean plate tectonics, which are defined by water cycling at 2–4% of modern rates that increase to modern values at 3 Ga. The dot–dash line indicates establishment of continental water cycling in the early Archaean while the solid line indicates establishment in the late Archaean. This plot highlights that there are no constraints on seawater  $\delta^{18}\text{O}$  during the Proterozoic eon from oceanic crustal rocks, so we assumed that  $\delta^{18}\text{O}$  of Proterozoic seawater resembled Phanerozoic seawater.

### 3. 早新元古代磷制约的海洋环境维持了较低大气氧含量



翻译人：蒋晓东 [jiangxd@sustech.edu.cn](mailto:jiangxd@sustech.edu.cn)

Guilbaud, R., Poulton, S.W., Thompson, J. et al., *Phosphorus-limited conditions in the early Neoproterozoic ocean maintained low levels of atmospheric oxygen*. *Nature Geoscience*. [J] (2020), 1–6.

**摘要：**在早新元古代（1-0.8 Ga），缺氧大陆边缘环境的氧化还原状态变化体现在由广泛的含硫化物状态转变为含铁氧化物状态。大洋的氧化还原条件对磷的生物地球化学循环具有很强的控制作用，由于磷是一种关键性的营养元素，因此对初级生产力也具有强控制力。然而目前磷循环对这种大尺度的海洋氧化还原环境转变的响应并不是很清楚。我们使用地球化学分类技术对开放大洋中不同相态的磷进行了研究，该样品取自中国北部淮南盆地早新元古代连续剖面。我们发现在含铁大洋中有效去除铁相矿物中生物可利用磷导致了贫营养环境，同时还很可能引起全球性的初级生产力、有机碳埋藏，以及随后的氧气生产量降低。虽然这样，但可利用磷和埋藏的有机碳足够维持大气氧化状态。这些数据暗示着在整个元古代营养元素驱动了大气氧含量变化，而不是通常认为的稳定的氧含量。

**ABSTRACT:** The redox chemistry of anoxic continental margin settings evolved from widespread sulfide-containing (euxinic) conditions to a global ferruginous (iron-containing) state in the early Neoproterozoic era (from ~1 to 0.8 billion years ago). Ocean redox chemistry exerts a strong control on the biogeochemical cycling of phosphorus, a limiting nutrient, and hence on primary production, but the response of the phosphorus cycle to this major ocean redox transition has not been investigated. Here, we use a geochemical speciation technique to investigate the phase partitioning of phosphorus in an open marine, early Neoproterozoic succession from the Huainan Basin, North China. We find that effective removal of bioavailable phosphorus in association with iron minerals in a globally ferruginous ocean resulted in oligotrophic (nutrient limited) conditions, and hence a probable global decrease in primary production, organic carbon burial and, subsequently, oxygen production. Nevertheless, phosphorus availability and organic carbon burial were sufficient to maintain an oxidizing atmosphere. These data imply substantial nutrient-driven variability in atmospheric oxygen levels through the Proterozoic, rather than the stable levels commonly invoked.

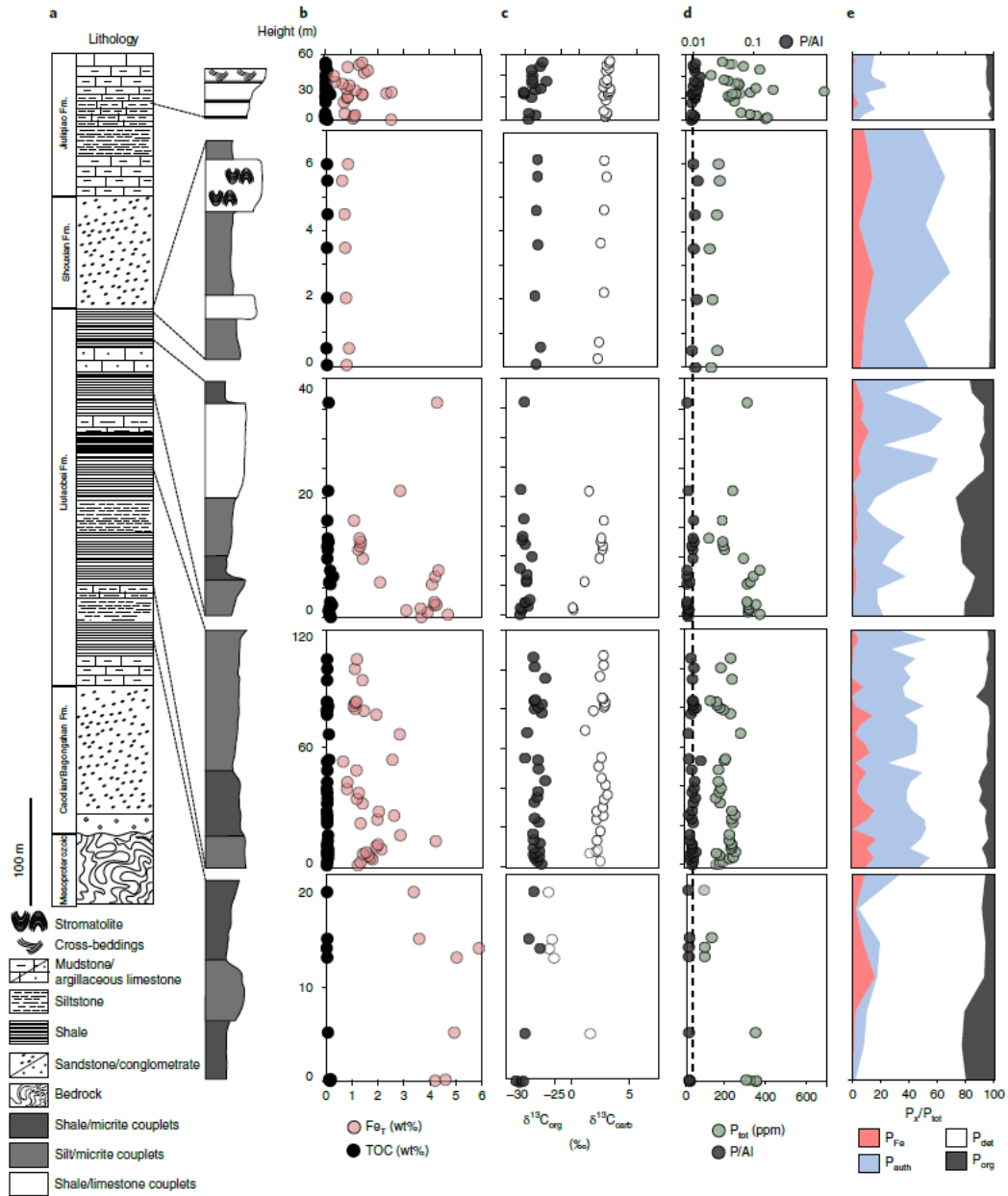


Figure 1. Geochemical variations against the main stratigraphy of the Huainan Basin. **a**, Stratigraphy of the Huainan Basin and lithology of the sections studied, modified after ref. 8. **b-e**, Geochemical variations: **b**, total organic carbon (TOC) and total Fe (Fe<sub>T</sub>) contents; **c**, organic carbon and carbonate carbon isotope compositions (δ<sup>13</sup>C<sub>org</sub> and δ<sup>13</sup>C<sub>carb</sub>, respectively); **d**, P<sub>tot</sub> contents and the P/Al ratio, the dotted line representing the average shale value<sup>38</sup> (note the difference in x axis); **e**, the proportion of P<sub>det</sub>, P<sub>auth</sub>, P<sub>org</sub> and P<sub>Fe</sub> within the total P pool. Errors are included within the data points.

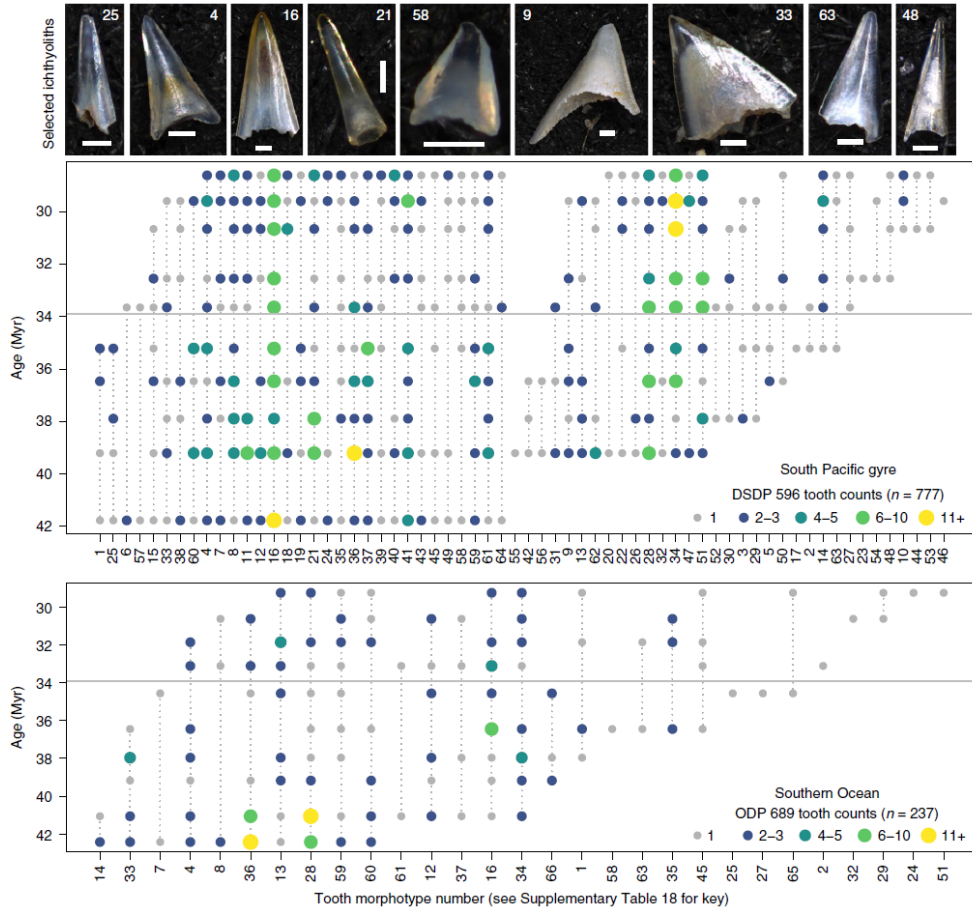


Figure 2. Biogeochemical evolution of the ocean at the Mesoproterozoic/Neoproterozoic boundary (ca. 1 Ga). **a**, Before ca. 1 Ga, mid-depth, euxinic (sulfide-rich,  $H_2S$ ) continental margins promoted P regeneration (as phosphate,  $PO_4^{3-}$ ) through preferential release from  $C_{org}$  and the reduction of Fe (oxyhydr)oxides, resulting in higher productivity and higher  $C_{org}$ -to- $P_{org}$  ratio. **b**, After ca. 1 Ga, under the globally ferruginous (Fe(II)-rich) early Neoproterozoic ocean, P was effectively removed from the water column and fixed in the sediment as authigenic phases through sink switching, resulting in oligotrophic continental margins and  $C_{org}/P_{org}$  close to the Redfield ratio.

#### 4. 晚新生代东南极洲和西南极洲的聚合

翻译人: 李园洁 liyj3@sustech.edu.cn



Granot R, Dymment J. *Late Cenozoic unification of East and West Antarctica*[J]. *Nature communications*, 2018, 9(1): 1-10.

**摘要:** 西南极洲裂谷系统的运动学演化过程对区域和全球性的动力学具有重要意义。但是, 由于缺乏新近纪板块边界的海底扩张, 以前研究认为东-西南极洲板块之间的运动中止于 26 Ma。本文我们在裂谷系统的北部边缘采集到的海洋磁异常数据表明东南极洲和西南极洲之间的相对运动一直持续到新近纪中期 (~11 Ma), 在中新生代的运动脉动停止之后的很长时间。我们计算了早新近纪的旋转参数, 为了解裂谷系统内的横贯南极山脉和构造-火山活动的不同的岩石圈背景提供运动学框架。将南极洲板块运动加入到全球板块回路对预测新近纪太平洋板块相对其他板块的运动具有重要的影响。

**ABSTRACT :** The kinematic evolution of the West Antarctic rift system has important consequences for regional and global geodynamics. However, due to the lack of Neogene seafloor spreading at the plate boundary and despite being poorly resolved, East-West Antarctic motion was assumed to have ended abruptly at 26 million years ago. Here we present marine magnetic data collected near the northern edge of the rift system showing that motion between East and West Antarctica lasted until the middle Neogene (~11 million years ago), long after the cessation of the known mid-Cenozoic pulse of motion. We calculate new rotation parameters for the early Neogene that provide the kinematic framework to understand the varied lithospheric settings of the Transantarctic Mountains and the tectono-volcanic activity within the rift. Incorporation of the Antarctic plate motion into the global plate circuit has major implications for the predicted Neogene motion of the Pacific Plate relative to the rest of the plates.

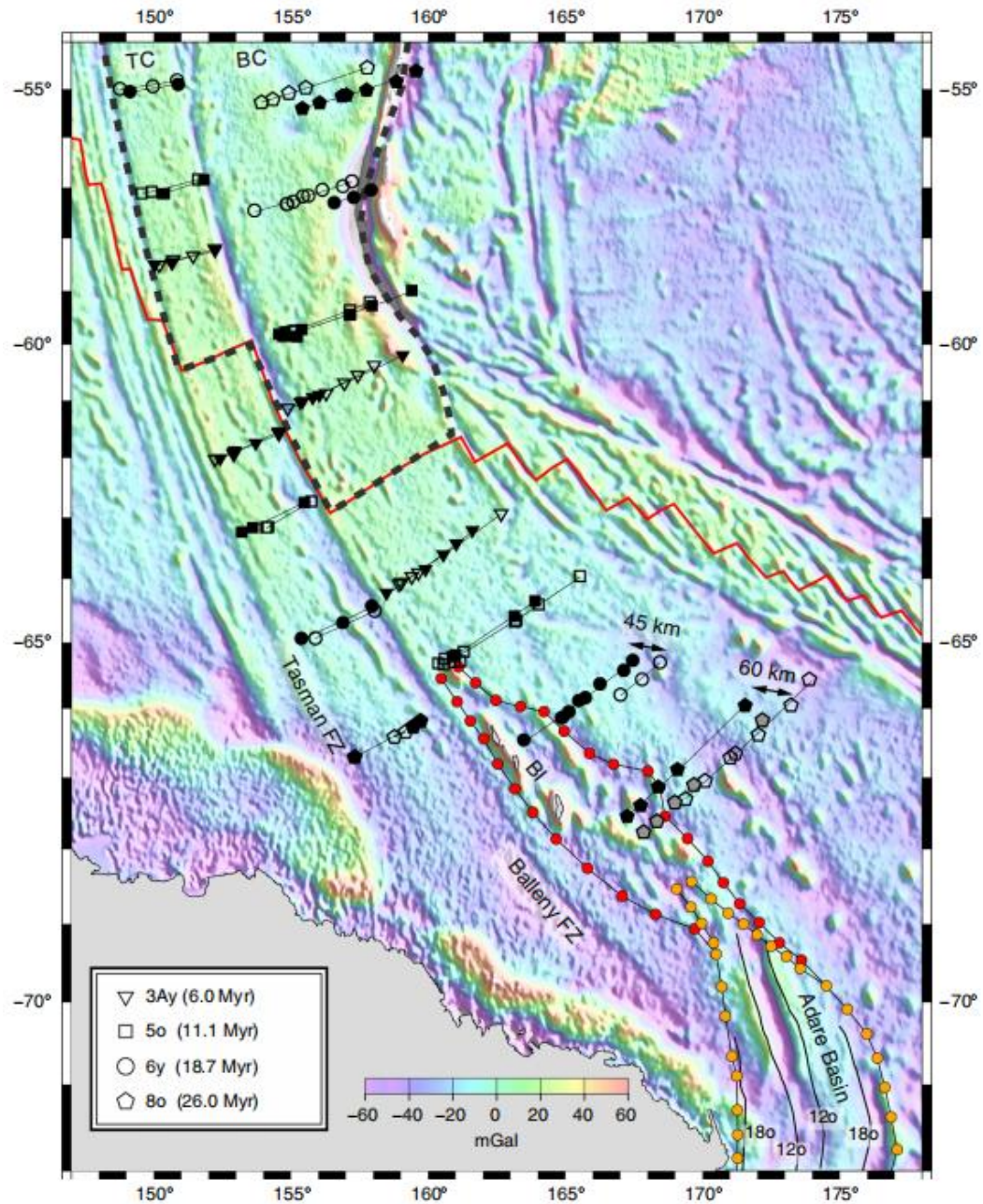


Figure 1. Magnetic anomaly locations in the Balleny and Tasman corridors. Background is the satellite-derived free-air gravity field. The positions of the anomalies (open symbols) are compared to those from the conjugate plate (filled symbols), rotated using the Australia-East Antarctica rotations. Anomalies from the Macquarie microplate, delineated by a dashed line, are corrected for Macquarie-Australia motion. Rotated anomalies 6y and 8o from the Balleny corridor misfit the positions of their Antarctic counterparts by 45 and 60 km, respectively. Grey-shaded anomaly picks (8o locations) are rotated using the Macquarie-Australia-West Antarctica rotation. Dotted red lines delineate the region of crust affected by Neogene East-West Antarctic motion. Dotted orange lines confine the Adare Basin with its internal anomalies 12o and 18o. BI, Balleny Islands; TC, Tasman corridor; BC, Balleny corridor.

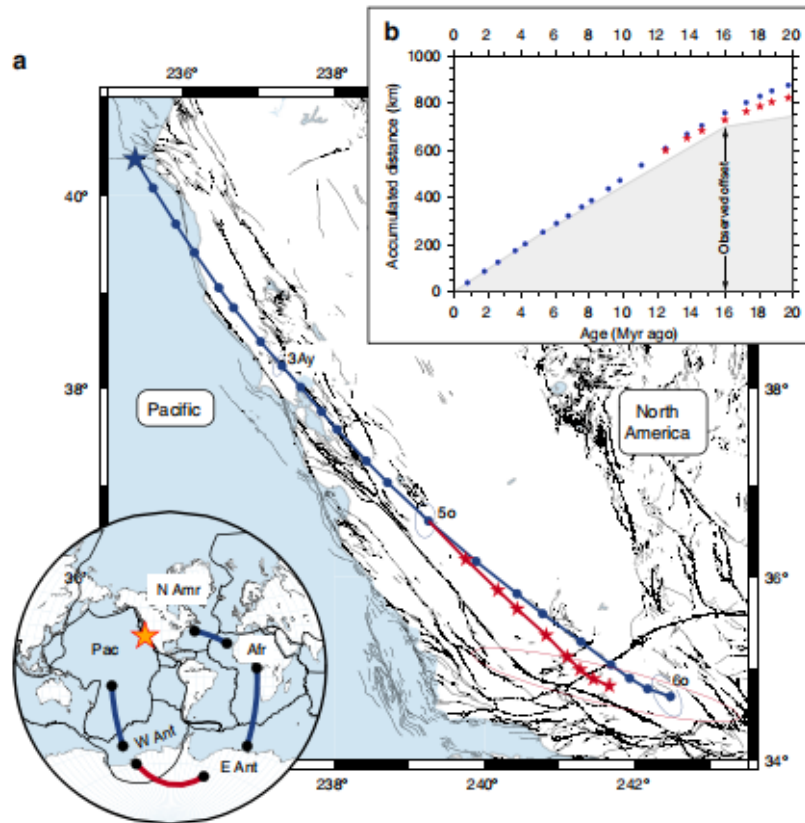


Figure 2. Pacific-North America plate motions during the Neogene. a Predicted plate motion trajectory for the Pacific Plate relative to the North America Plate. The blue line shows the trajectory calculated by the summation of the noise-reduced Pacific-Antarctica-Africa-North America plate circuit rotations, assuming that Antarctica was a single plate. Inclusion of East-West Antarctica motion between anomalies 80 and 50 results in the red trajectory. Ellipses show the resulting combined 95% uncertainty region for the reconstructed Mendocino Triple Junction (blue star). b Accumulated boundary-parallel displacement components (N40°W direction) calculated along the trajectories shown in panel a (blue and red stars were computed excluding and including, respectively, Neogene East-West Antarctica motion). Geological estimates of the boundary-parallel displacements across the plate boundary are shown by gray shaded area.

## 5. 湖泊沉积物中碳酸盐岩的稳定氧碳同位素作为古洪水的代用指标



翻译人：郑威 11930589@mail.sustech.edu.cn

Kämpf L, Plessen B, Lauterbach S, et al. *Stable oxygen and carbon isotopes of carbonates in lake sediments as a paleoflood proxy*[J]. *Geology*, 2020, 48(1): 3-7.

**摘要：**湖泊沉积物越来越多地被视为记录古洪水的可靠档案。除了已建立的包括碎屑层厚度、化学成分、粒度等洪水代用指标外，我们探究了稳定氧碳同位素数据作为基岩为碳酸盐岩的流域中湖泊的古洪水代用指标。在奥地利Mondsee湖的案例研究中，我们整合了近端和远端收集的高分辨率沉积物和有纹层的湖泊沉积物钻孔的稳定同位素分析以研究洪水触发的碎屑沉积物的通量。首先，我们证明了公元2011-2013年间径流量、碎屑沉积物通量与沉积物记录的同位素数值之间的关系，包括了22个事件，其径流量日（小时）峰值为10（24） $\text{m}^3\text{s}^{-1}$ 到79（110） $\text{m}^3\text{s}^{-1}$ 。远端收集的沉积物中减弱的稳定同位素数值的峰值很好的反映了3-10倍少的洪水触发的碎屑沉积物在远端沉积。接下来，我们表明，沉积物记录的1988-2013年间所有9层洪水触发的碎屑层与内生的方解石相比有较高的同位素数值。此外，尽管有两个径流事件没有造成可见的碎屑层沉积也通过较高的同位素数值显示出来。同位素数据的经验阈值可以估算大多数洪水的强度，尽管在某些案例中洪水强度因为区域影响导致了过高的同位素数值而被高估了。因此，我们提出了一个稳定同位素作为重建洪水频率的可靠工具的概念的证明，但是它依然存在一些甚至是对洪水强度的估计的局限性。

**ABSTRACT:** Lake sediments are increasingly explored as reliable paleoflood archives. In addition to established flood proxies including detrital layer thickness, chemical composition, and grain size, we explore stable oxygen and carbon isotope data as paleoflood proxies for lakes in catchments with carbonate bedrock geology. In a case study from Lake Mondsee (Austria), we integrate high-resolution sediment trapping at a proximal and a distal location and stable isotope analyses of varved lake sediments to investigate flood-triggered detrital sediment flux. First, we demonstrate a relation between runoff, detrital sediment flux, and isotope values in the sediment trap record covering the period 2011–2013 CE including 22 events with daily (hourly) peak runoff ranging from 10 (24)  $\text{m}^3\text{s}^{-1}$  to 79 (110)  $\text{m}^3\text{s}^{-1}$ . The three- to ten-fold lower flood-triggered detrital sediment deposition in the distal trap is well reflected by attenuated peaks in the stable isotope values of trapped sediments. Next, we show that all nine flood-triggered detrital layers deposited in a sediment record from 1988

to 2013 have elevated isotope values compared with endogenic calcite. In addition, even two runoff events that did not cause the deposition of visible detrital layers are distinguished by higher isotope values. Empirical thresholds in the isotope data allow estimation of magnitudes of the majority of floods, although in some cases flood magnitudes are overestimated because local effects can result in too-high isotope values. Hence we present a proof of concept for stable isotopes as reliable tool for reconstructing flood frequency and, although with some limitations, even for flood magnitudes.

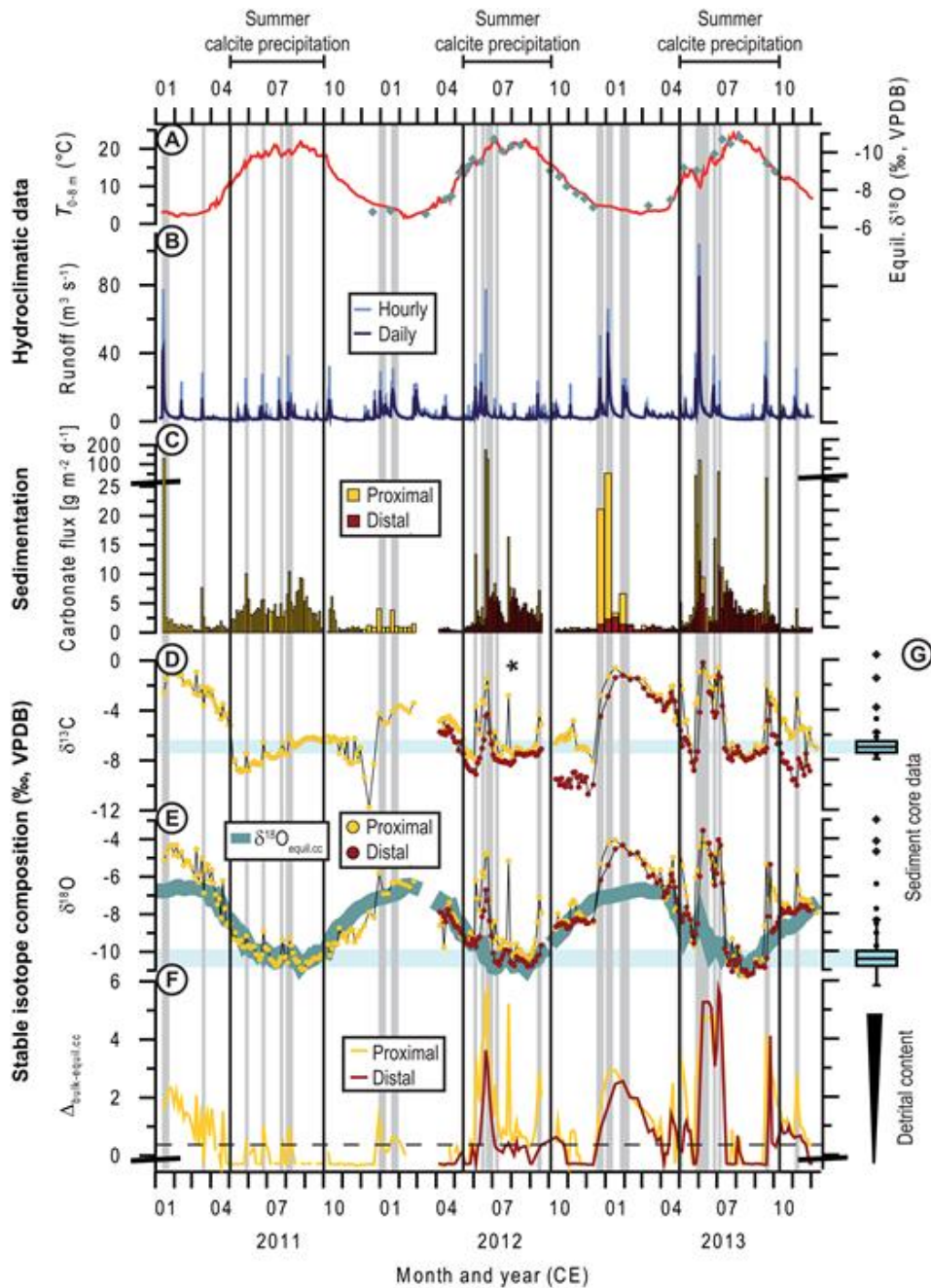


Figure 1. Three years of monitoring data on hydroclimatic variables and trapped sediment at Lake Mondsee (Austria). Gray vertical bars mark flood-triggered peaks in sediment flux and isotopes. (A)

Epilimnion (0–8 m depth) water temperature (red line) and calculated equilibrium  $\delta^{18}\text{O}$  (green diamonds) of endogenic calcite (Appendices DR1 and DR2 [see footnote 1]). (B) River runoff. (C) Carbonate flux. Note change in vertical scale above  $25 \text{ g m}^{-2} \text{ d}^{-1}$ . (D) Bulk  $\delta^{13}\text{C}$  in sediment. Star marks one isotope peak not correlated to runoff due to gap in runoff data. (E) Bulk  $\delta^{18}\text{O}$  in sediment with calculated endogenic calcite  $\delta^{18}\text{O}$  ( $\delta^{18}\text{O}_{\text{equil.cc}}$ ) (Appendix DR2). (F) Differences between measured and calculated endogenic  $\delta^{18}\text{O}$  ( $\Delta_{\text{bulk-equil.cc}}$ ). Horizontal dashed line marks the minimum difference between measured  $\delta^{18}\text{O}$  and  $\delta^{18}\text{O}_{\text{equil.cc}}$  (0.5 per mil). (G) Bulk  $\delta^{13}\text{C}$  and  $\delta^{18}\text{O}$  of calcite layers (box plots,  $n = 17$ ), microscopic detrital layers (dots,  $n = 9$ ), and macroscopic detrital layers (diamonds;  $n = 3$ ). “Proximal” and “distal” indicate proximal and distal sediment traps, respectively (see Fig. 1). VPDB—Vienna Peedee belemnite.

## 6. 海洋中金属元素在生物和非生物作用下的滞留、再循环和矿化过程



翻译人：王敦繁

Boyd P W, Ellwood M J, Tagliabue A, et al. *Biotic and abiotic retention, recycling and remineralization of metals in the ocean*[J]. *Nature Geoscience*, 2017, 10(3):167-173.

**摘要:** 海洋中的生物地球化学循环过程以及海洋中的生物生态结构都与微量元素密切相关，目前人们对海洋中微量元素生物地球化学过程的研究主要聚焦在其外源输入模式上，比如粉尘输入，热液活动以及沉积作用等。然而，海洋中的金属元素也存在其内部的转化过程，比如在生物或非生物作用下的滞留，再循环以及矿化过程。人们现在对金属元素生物地球化学作用的研究也越来越关注其在内部的转化过程。首先，在生物作用下金属元素在海水表层的滞留时间可达数天或数周甚至数月，并由浮游生物所能够利用的元素种类和其最终归宿所决定，比如从病毒溶解到赋存时间再到被捕食并最终输送到海底。相比单独的外源输入，海洋表层金属元素快速的再循环作用更能通过保持高水平的生物可利用性促进其季节性的生产力水平。随着含金属元素的有机颗粒从海洋表面输送下来，不同的金属元素在不同深度表现出不同的再矿化模式。这些模式是由一系列广泛的物理化学和微生物过程调节的，比如颗粒吸附金属的能力，以及沉降颗粒的矿物和有机特征。研究表明金属元素的内部转化过程在控制金属的生物利用度、浮游植物分布以及深部金属元素再补给方面起着重要作用。

**ABSTRACT:** Trace metals shape both the biogeochemical functioning and biological structure of oceanic provinces. Trace metal biogeochemistry has primarily focused on modes of external supply of metals from aeolian, hydrothermal, sedimentary and other sources. However, metals also undergo internal transformations such as abiotic and biotic retention, recycling and remineralization. The role of these internal transformations in metal biogeochemical cycling is now coming into focus. First, the retention of metals by biota in the surface ocean for days, weeks or months depends on taxon-specific metal requirements of phytoplankton, and on their ultimate fate: that is, viral lysis, senescence, grazing and/or export to depth. Rapid recycling of metals in the surface ocean can extend seasonal productivity by maintaining higher levels of metal bioavailability compared to the influence of external metal input alone. As metal-containing organic particles are exported from the surface ocean, different metals exhibit distinct patterns of remineralization with depth. These

patterns are mediated by a wide range of physicochemical and microbial processes such as the ability of particles to sorb metals, and are influenced by the mineral and organic characteristics of sinking particles. We conclude that internal metal transformations play an essential role in controlling metal bioavailability, phytoplankton distributions and the subsurface resupply of metals.

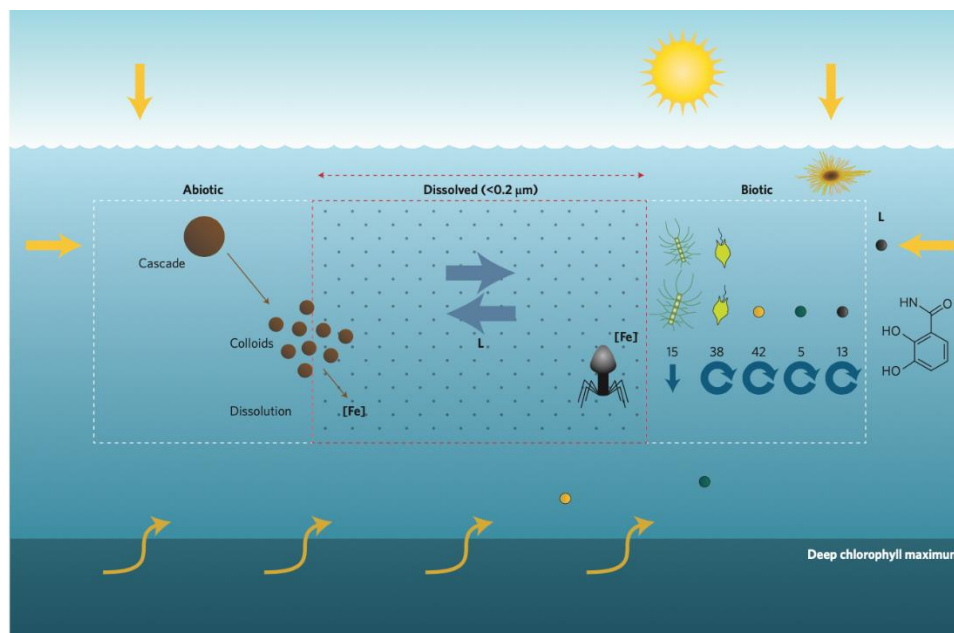


Figure 1: Schematic of modes of ‘new’ iron supply (orange arrows) and iron retention mechanisms within the surface mixed layer. Abiotic retention (left box) includes rapid transfer of aerosol iron to soluble pools (that is, Cascade<sup>7</sup>) and photochemically mediated colloid dissolution<sup>34</sup>. Biotic retention (right box) is driven by acquisition (for example, aerosol capture by diazotrophs<sup>36</sup>) and interactions between iron supply, differing iron quotas (pmol l<sup>-1</sup>) within natural communities (left-to-right: diatom<sup>39</sup>, autotrophic flagellate<sup>39</sup>, picoprokaryote<sup>39</sup>, picoeukaryote<sup>39</sup>, heterotrophic bacterium<sup>39</sup>) and their fate (export (downward blue arrow) or grazing/lysis (circular blue arrows)). Microbial ligand (L) release retains metals in solution (denoted by the partial chemical structure of the enterobactin siderophore) and is stimulated by new metal supply<sup>25,26</sup>. The virus represents putative iron recycling through progeny phages<sup>33</sup>. Horizontal blue arrows denote exchange between the dissolved and other pools mediated by ligands.

## 7. 中国降水的稳定同位素组成



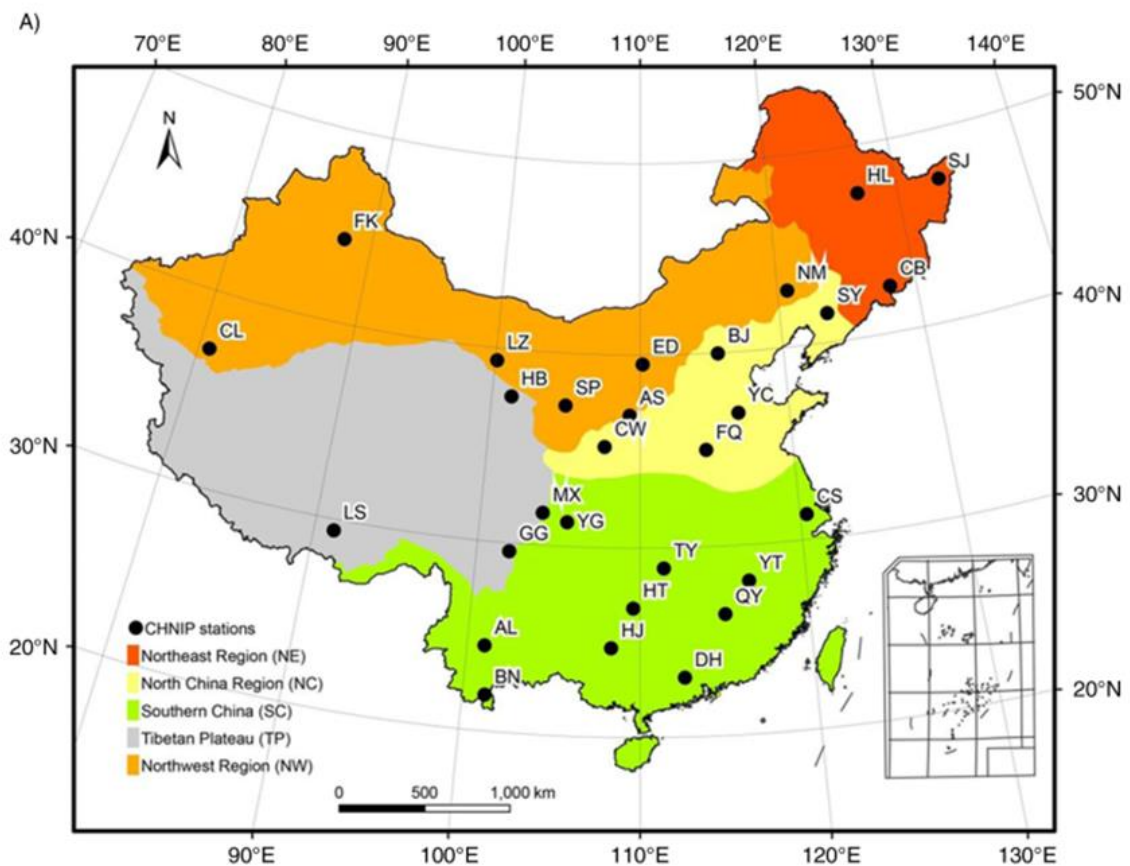
翻译人: 杨会会 11849590@mail.sustech.edu.cn

Liu J R, Song X F, Yuan G F, et al. *Stable isotopic compositions of precipitation in China [J]. Tellus B*, 2014, 66, 22567.

**摘要:** 二十世纪八十年代中期, 中国有 31 个观测站成功参与了全球降水同位素网络。然而九十年代中期以后, 大部分观测数据可靠性存疑。不连续的数据阻碍了应用降水同位素值, 降水同位素在中国受亚洲季风的强烈影响, 这引起了古气候学家的兴趣。因此, 为了全国范围地连续观测降水同位素值, 2004 年建立了中国降水同位素网络。本次研究回顾了 2005 年至 2010 年收集的 928 个样本的主要特征。D 和 O 同位素值变化范围遵循以下顺序: NE>NW>TP>NC>SC, 加权同位素值变化遵循的顺序为: SC>NW>NC>TP>NE。时间序列上的变化, 在华南地区呈现“V”型, 在东北和西北地区呈现反“V”型, 在华北和青藏地区随雨季的到来呈现降低趋势。中国雨量曲线已经建立起来了,  $dD=7.48d^{18}O+1.01$ 。沿曲线散点的分布表明不同类型水蒸气的来源和特征。 $d^{18}O$  值在西北和东北地区表现出与温度的强相关性 ( $0.27\text{‰}/^{\circ}\text{C}$  和  $0.37\text{‰}/^{\circ}\text{C}$ ), 而在华南地区则受水汽压和大气压变化的影响。氧同位素在纬度上变率为  $-0.22\text{‰}/^{\circ}\text{C}$ , 在海拔上是  $-0.13\text{‰}/100\text{m}$ 。氧同位素/纬度这一梯度在东部季风区由南向北逐渐增加, 氧同位素/海拔 ( $-0.30\text{‰}/100\text{m}$ ) 在青藏高原地区尤其显著。本次研究结果为全国不同地区正在进行的水文学、气象学、古气候学和生态学调查提供了基础的同位素信息。

**ABSTRACT:** During the mid-1980s, there were 31 stations in China that successfully participated in the Global Network of Isotopes in Precipitation. However, most observations were suspended after the mid-1990s. The discontinuous data hindered the application of precipitation isotopes, which are strongly affected in China by the Asian monsoon and are thus of intrinsic interest for palaeoclimatologists. Therefore, to continuously observe precipitation isotopes nationwide, the Chinese Network of Isotopes in Precipitation was established in 2004. The current study reviewed the major characteristics of the 928 samples that were collected from 2005 to 2010. The ranges of  $dD$  and  $d^{18}O$  values generally followed the pattern NENWTPNCSC, and the amount weighted  $d$ -values followed the pattern SCNWNCTPNE. Temporal variations presented a ‘V’-shaped pattern

at the SC region and reverse ‘V’-shaped patterns at the NE and NW regions. Decreasing trends with the advent of the rainy season were found at the NC and TP regions. The Chinese Meteoric Water Line has been established as  $dD=7.48d^{18}O + 1.01$ . The distributions of scattering along the line demonstrated different water vapor origins and characteristics. The values of  $d^{18}O$  showed strong temperature dependence at the NE ( $0.27\text{‰}/^{\circ}\text{C}$ ) and NW stations ( $0.37\text{‰}/^{\circ}\text{C}$ ), and this dependent variable switched to water vapor pressure and vapor pressure at the SC stations. The geographical controls of  $d^{18}O$  were  $-0.22\text{‰}/^{\circ}$  and  $0.13\text{‰}/100\text{ m}$  for latitude and altitude, respectively. The  $d^{18}O$ /Latitude gradient increased from south to north at the Eastern Monsoon Region, and the  $d^{18}O$ /Altitude gradient ( $-0.30\text{‰}/100\text{ m}$ ) was especially significant for the TP region. The results of this study could provide basic isotopic information for on-going investigations in hydrology, meteorology, palaeoclimatology and ecology at different regions of China.



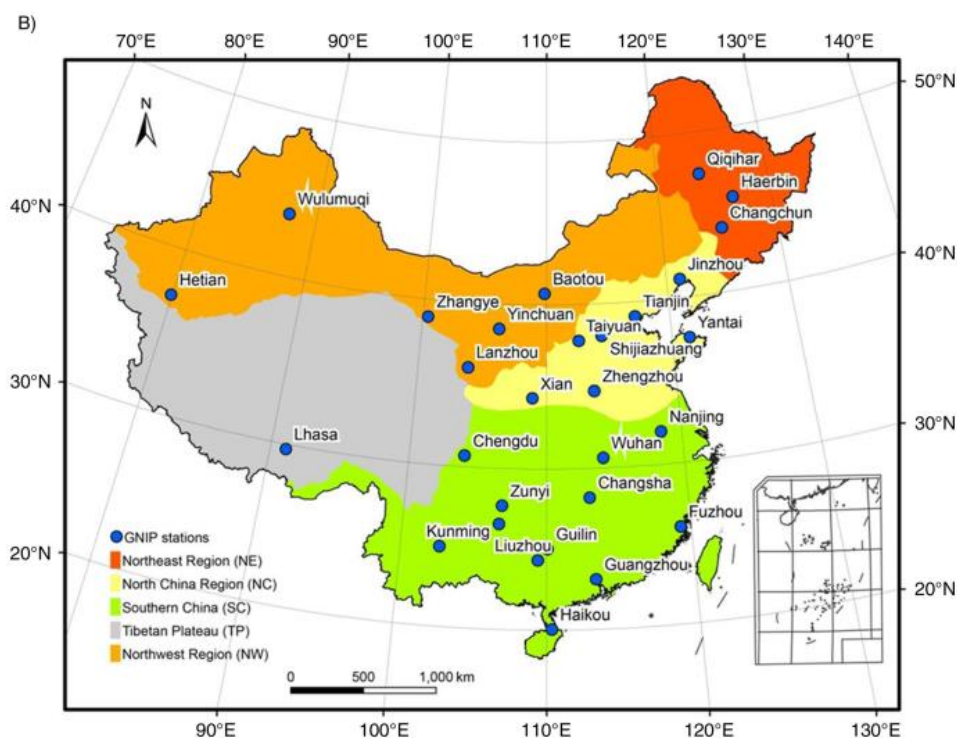


Figure 1. Locations of (a) CHNIP stations and (b) GNIIP stations.

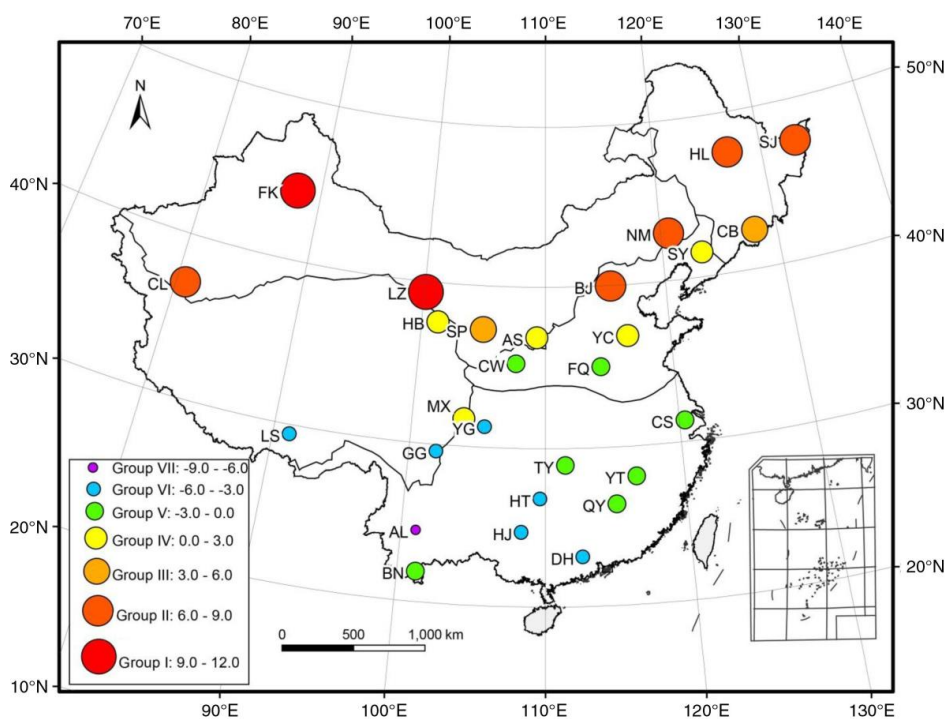


Figure 2. Distributions of  $(\delta_s - \delta_w)$  values. The  $\delta_s$  and  $\delta_w$  denote the un-weighted means of the summer (May-Oct.) and winter months (Nov.-Apr.), respectively. Group I, II and III all belong to the inner continental climate, indicating a major temperature contribution to the  $d^{18}O$  variation. Group IV and V are generally located in the middle and southeastern parts of China, and both the precipitation and temperature may contribute to the small  $(\delta_s - \delta_w)$  values. Group VI and VII distribute to latitude  $< 30^\circ N$ , and with a precipitation contribution.

## 8. 全新世以来南海北部海岸海表温度变化所指示的亚洲冬季季风记录



翻译人: 王浩森 502691781@qq.com

Zhang Y, Zhu K, Huang C, et al. 2019. *Asian Winter Monsoon Imprint on Holocene SST Changes at the Northern Coast of the South China Sea*. 46: 13363-13370.

**摘要:** 尽管在几个地区获得了亚洲冬季季风 (AWM) 的结果, 但关于全新世的可变性尚未达成共识。以中国南海北部海岸 (SCS) 的沉积物来分析 10 (20) 年分辨率的有机生物标志物, 揭示了 SCS 得海洋条件如何指示 AWM 信号。一般而言, 海表温度 (SST) 记录类似于过去 7500 年以来热带地区海表温度的时间结构, 显示了小冰期和 1200~2500 年 BP 之间异常的低温 (最高 ~4°C)。风生陆源烷类化合物显著增加时, 其叠加趋势也是总体增加。结果显示, 随着南海海岸和开阔海洋之间海表温度梯度的增加, AWM 在晚全新世之前不断加强。在类似小冰河期这样的冷期中增强的 AWM 将提供强大的正反馈, 以增强沿海降温过程。

**ABSTRACT:** Independent inference of the Asian winter monsoon (AWM), albeit achieved at several sparse sites, has reached no consensus for its variability through the Holocene. A sediment core from the northern coast of the South China Sea (SCS) was utilized to analyze organic biomarkers at (bi-)decadal resolution, unveiling how SCS oceanic conditions fingerprint the AWM signal. Generally, alkenone sea surface temperature (SST) record, resembling the temporal structures of integrated tropical SST over the past 7,500 years, shows abnormal cool temperatures (up to ~4 °C) during the Little Ice Age and between ~1,200 and 2,500 years BP, when windborne terrigenous hopane compounds experienced considerable increases superimposed on a general increasing trend. Our results, together with augmented SST gradient between the SCS coast and open ocean, consistently suggest AWM strengthening toward the late Holocene. An intensified AWM during cold intervals like the Little Ice Age would have provided strong positive feedback to enhance coastal cooling.

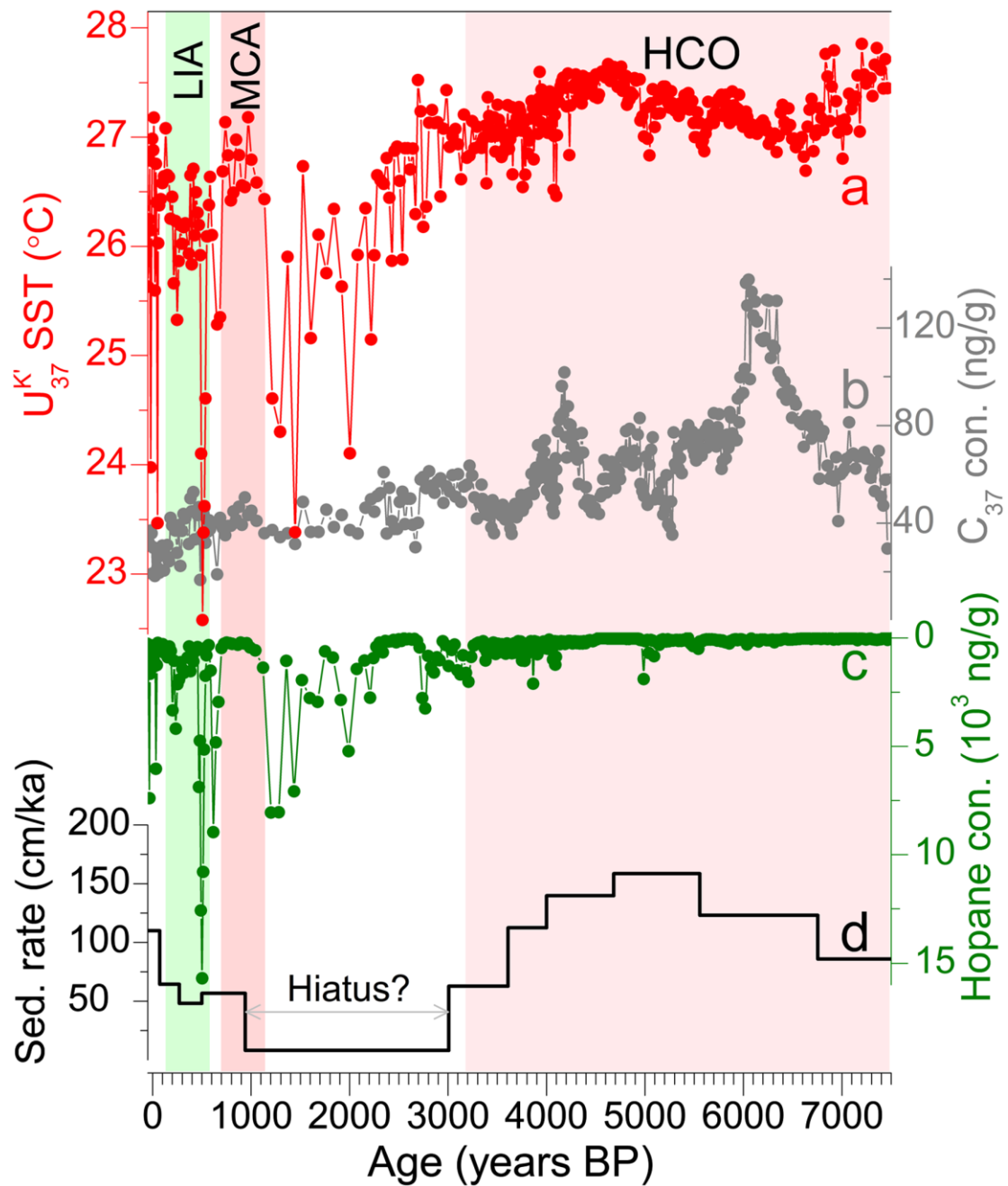


Figure 1. Downcore geochemical proxies of sediment core YJ over the past 7,500 years, including (a)  $U^{K}_{37}$ -SST record, (b)  $C_{37}$  concentration, (c) total hopane concentration (reversed scale), and (d) sedimentation rate. The color bars represent three key intervals discussed in the text, for example, the Holocene Climate Optimum (HCO, before ~3,500 years BP), Medieval Climate Anomaly (MCA, ~700–1100 years BP) (red), and Little Ice Age (LIA, ~150–550 years BP) (green).

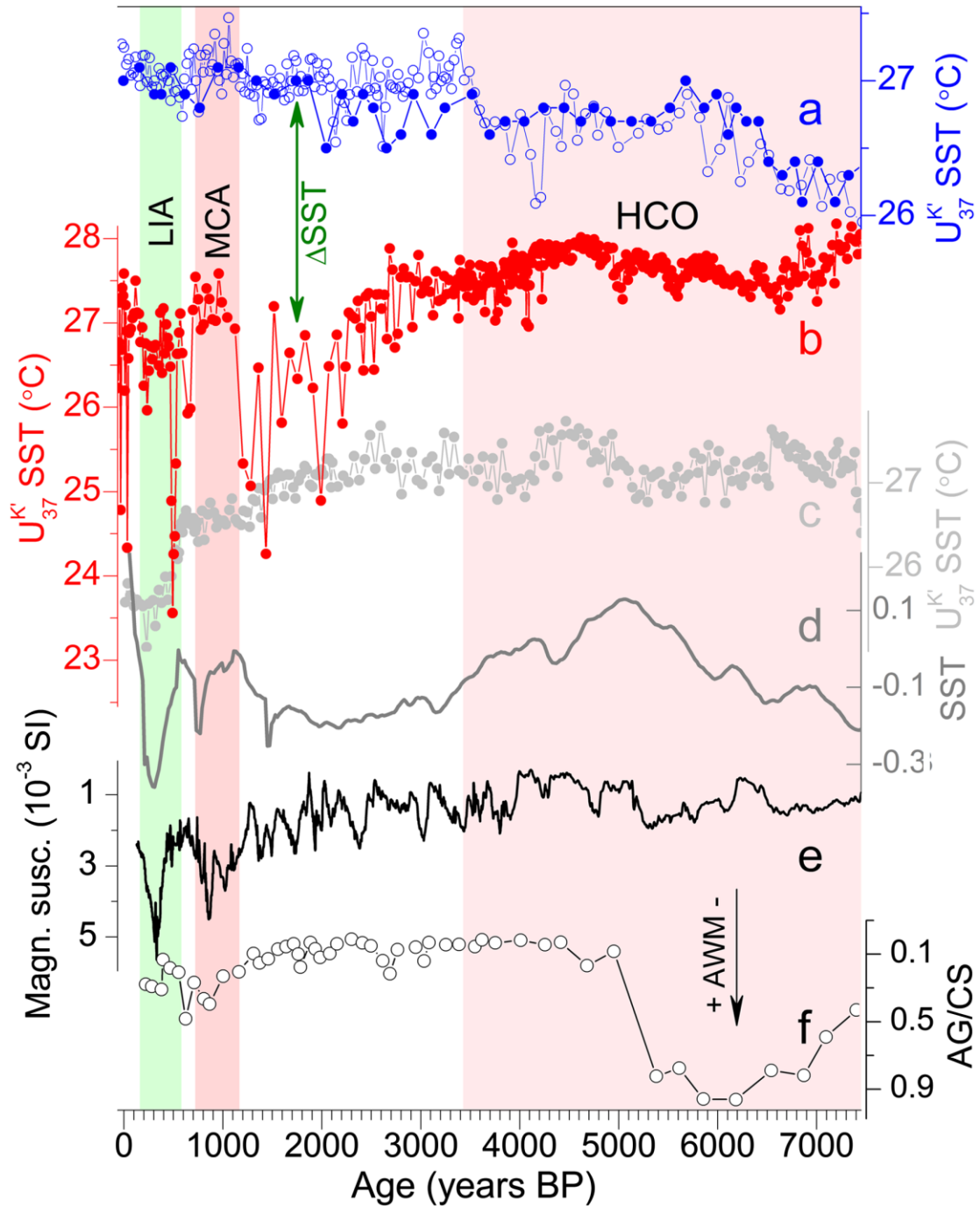


Figure 2. Comparison of  $U^{K}_{37}$ -SST records of sediment cores (a) GIK17940 (blue dots) (Wang et al., 1999) and NS02G (blue cycles) (Kong, 2014), (b) YJ (this study), and (c) HKUV16 (Kong et al., 2014), (d) integrated SST anomaly over global tropical coasts (Marcott et al., 2013) as well as (e) magnetic susceptibility (values increase downward, Yancheva et al., 2007) and (f) diatom AG/CS ratio (*A. granulate*/*C. stelligera*; Wang et al., 2012) at Huguangyan Maar Lake. The color bars mark the same intervals as in Figure 2, and the green arrow line denotes the SST gradient between the SCS northern coast and open ocean.

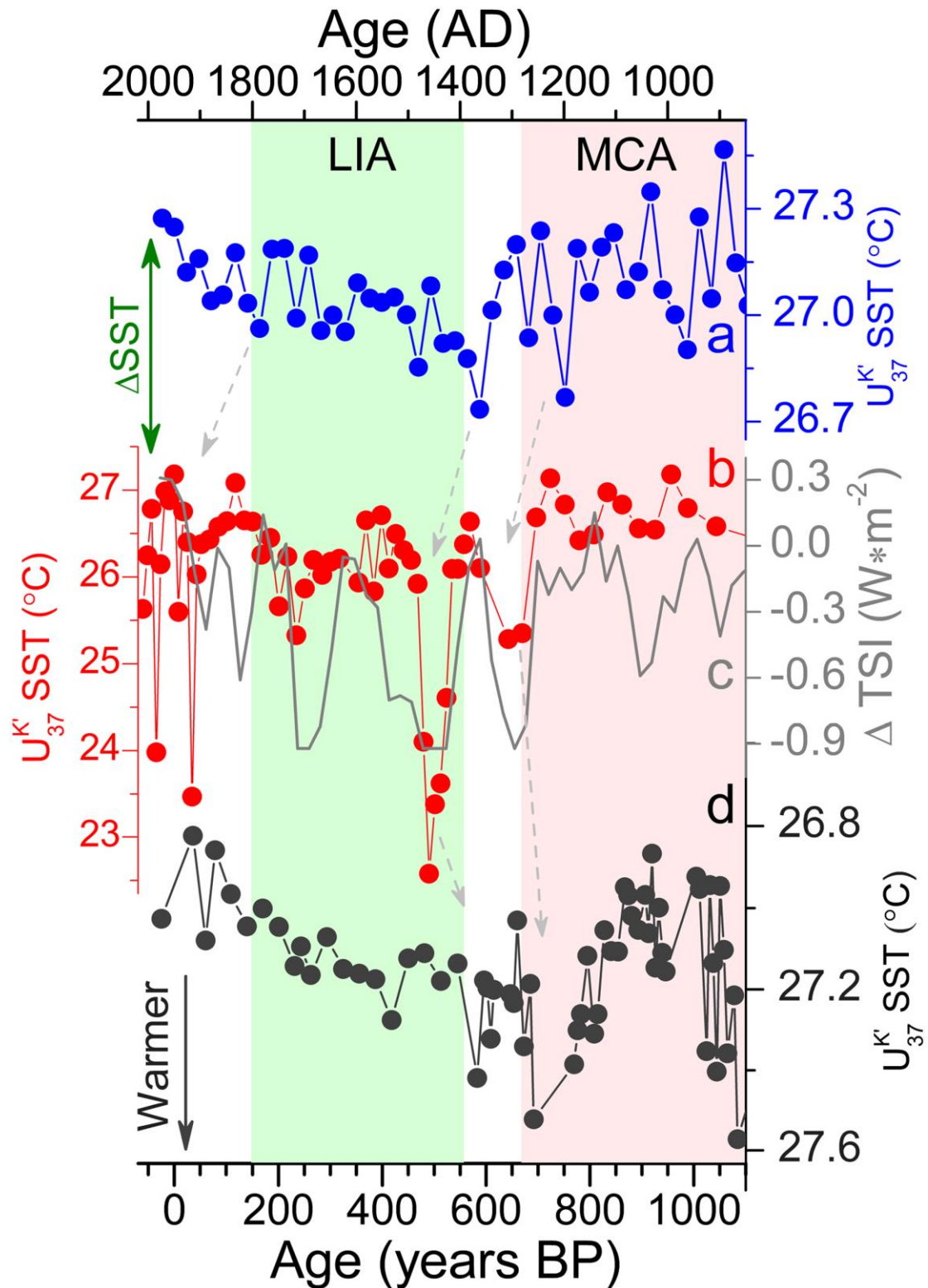


Figure 3. Comparison of  $U_{37}^K$ -SST records over the last millennium in sediment cores (a) NS02G (Kong et al., 2017), (b) YJ (this study), and (d) HKGS-A (higher values downward) (Lee et al., 2019). The color bars and green arrow line outline the same intervals and SST gradient, respectively, as in Figure 3, and the dashed gray lines hint at the correspondence of three independent records within their chronological uncertainties. Total solar irradiance (TSI) (Steinhilber et al., 2009) is also superimposed upon the SST record (c). Note different temperature scale used for the three records.